

Study of Catalytic Potency of Green Synthesized AgO Nanoparticles in the Degradation of Oxcarbazepine by Chloramine-T in Acidic Aqueous Medium

H.S. SONAKSHI[✉], M.K. ARPITHA[✉], K.M. VIDYASHREE and H.P. JAYADEVAPPA^{*✉}

Department of Chemistry, Yuvaraja's College, University of Mysore, Mysuru-570006, India

*Corresponding author: E-mail: hpjayadevappa@gmail.com

Received: 14 August 2024;

Accepted: 20 December 2024;

Published online: 31 January 2025;

AJC-21881

The current paper deals with the green synthesis of AgO nanoparticle by sol-gel method and their characterization. Kinetic, mechanistic and thermodynamic studies of AgO nanoparticles catalyzed and uncatalyzed oxidation of oxcarbazepine (OXC) by chloramine-T (CAT) in acidic aqueous medium at 298 K. The stoichiometric parameters of reaction were determined, enabling the identification of the oxidation products for both uncatalyzed and nanoparticle AgO catalyzed reactions. The determined reaction rate exhibited first order dependence on [oxidant] for uncatalyzed reaction whereas non-integer order dependence on nanoparticle catalyzed reaction. The course of reaction shows non-integer order dependence was found on both [OXC] and [H⁺]. Further rates of reactions were almost unaffected by the products of reaction. A minor inhibitory impact of the dielectric constant was observed for both AgO nanoparticle-catalyzed and uncatalyzed reactions. The reaction rate remained invariant with changes in ionic strength, suggesting the participation of non-ionic species in the rate-determining step. Free radical intermediates were not detected during the course of the reaction. A series of kinetic runs were performed at various temperatures (298-313 K) to evaluate thermodynamic parameters. The experimental data were used to develop a mechanism consistent model, from which the rate laws were derived.

Keywords: Kinetics, Chloramine-T, Oxcarbazepine, Degradation, Rate law, AgO nanoparticle, Stoichiometry.

INTRODUCTION

Oxcarbazepine, a novel antiepileptic agent having chemical name 5-oxo-6H-benzo[b][1]benzazepine-11-carboxamide, represents a second-generation advancement over carbamazepine. Oxcarbazepine (OXC) is structurally related to carbamazepine and is having anticonvulsant property, which performs by reducing abnormal electric activity in brain [1,2]. The anticonvulsant activity of OXC is mediated by blocking the neuronal ion channels [3-6]. The OXC extended-release drugs are used with supplementary medications to control certain kinds of specific seizures in elders and pediatric patients of 6 years and above [7-9].

Aryl N-halosulfonamides have diverse properties and reacts with varieties of functional groups and hence used as versatile reagents in performing a number of transformations [10]. The presence of strongly polarized N-linked halogen in the +1 oxidation state imparts mild oxidizing properties to these compounds in both alkaline and acidic solution. As precursors to hypohalite, halonium species and nitrogen anions, these compounds

exhibit reactivity characteristic of bases and nucleophiles [11]. Aromatic sulphonyl halo amines display multifaceted properties, serving as both oxidant and halogenation reagents in various chemical reactions. Moreover, these compounds are also employed as analytical reagents for the quantitative determination of various reducing agents in solution [12]. Among the members of organic haloamine family, N-chloro-*p*-toluene sulfonamide, widely recognized by its trade name chloramine-T (CAT), is a significant chemical entity. CAT is the major species, demonstrating effective oxidation capabilities in a wide pH range, encompassing both acidic and basic conditions [13]. The oxidative properties of organic haloamines are reminiscent of those displayed by hypohalites, but they offer the advantage of enhanced stability. It has great biological importance as an antimicrobial agent [14]. As a notable member of the organic haloamine class, CAT engages in a variety of reactions with different functional groups, enabling numerous molecular transformations, with many of its kinetic and mechanistic aspects having been elucidated [15-22].

Transition and inner-transition metal ions exhibit catalytic behaviour by forming unstable intermediates with the reactants multiple oxidation states due to the presence of unoccupied *d*- and *f*-orbital, which allow them for flexible electron configuration. Silver oxide (AgO) nanoparticle is an effective catalyst for various oxidative processes including N_{ox} reduction, formaldehyde production, oxidation of benzyl alcohol, ethylene epoxidation, electron transfer reactions of styrene, ethylene glycol and CO also catalytic transformation of NH_3 . The efficacy of silver nanoparticle catalysts is predominantly influence by their surface topology and compositional characteristics. The incorporation of AgO nanoparticles into the catalyst enhances the area of exposure and increases the density of active sites, thereby augmenting catalytic activity [23,24].

A comprehensive review of the literature on oxcarbazepine reveals key aspects of drugs including quantitative determinations methods, biodegradation processes, mechanism of action. Degradation of oxcarbazepine by mild oxidants and nanoparticle catalyzed has not been reported yet. In present communication, we are reporting the kinetics of AgO nanoparticles catalyzed and uncatalyzed reactions of oxcarbazepine by chloramine-T (CAT) and its related mechanistic and thermodynamic aspects in acidic aqueous medium at 298 K.

EXPERIMENTAL

The chemicals and reagents utilized for the experiment were of analytical reagent grade unless specified. Double-distilled water was employed as solvent for the kinetic studies. A stock solution of potassium nitrate was prepared by dissolving the salt in double distilled water and this solution was used directly to maintain the desired ionic strength. Various amount of methanol was added to the reaction solution to obtain the right dielectric properties. Double-distilled water was used consistently as solvent for preparing solutions to maintain reproducibility.

Synthesis of Silver oxide nanoparticle

Sol-gel synthesis: About 5 g of dried leaves of papaya was added to 100 mL of double distilled water and boiled for about 3 h continuously and then filtered. About 2.5 g of silver nitrate was dissolved in 50 mL of double distilled water and kept in 800 rpm magnetic stirrer for about 0.5 h then the papaya leaves extract was added followed by 5 mL of 1:1 ammonia solution to maintain basic pH of the medium. The extraction process was optimized through 4 h heat treatment to the mixture with constant stirring at 900 rpm. Subsequent processing steps, including cooling, centrifugation, washing with deionized water and ethyl alcohol and drying in an oven at 100 °C for 10 h using an incubator, resulting in the successful isolation of the desired precipitate.

An aqueous solution of chloramine-T (CAT) was carefully prepared in double-distilled water. It was standardized by the iodometrically and preserved in the Amber glass bottle so as to prevent further deterioration photochemically. An aqueous solution of oxcarbazepine (OXC) substrate was prepared immediately before use to the desired concentration prior to each

experiment. Required weight of AgO nanoparticles catalyst was used in the reaction mixture for the catalyzed reaction.

Kinetic measurements: To facilitate the analysis of kinetic data, the pseudo-first-order conditions were established by maintaining a significant excess of [OXC] over the catalyst [CAT] in both catalyzed and uncatalyzed experiments. A reaction mixture was prepared by combining precise volumes of OXC, HCl and NaCl solutions in a sealed Pyrex tube with a glass stopper, facilitating subsequent kinetic analysis. A requisite volume of water was added to maintain a constant total volume across all the experimental runs. The reaction mixture was thermostatic at 298 K for sufficient time. A pre-equilibrated solution of the CAT was added to the mixture in the requisite amount, followed by thorough agitation. For the nanoparticle catalyzed reaction, a known amount of AgO nanoparticle was added. Immediately pipetted out and poured into the reaction flask containing ice cold water. Iodometric analysis was utilized to track the reaction progress by estimating the unreacted CAT concentration in 2 mL samples of the reaction mixture at the regular time intervals, enabling the determination of the kinetic parameter of the reaction. A reproducibility of $\pm 3\%$ was observed for the pseudo-first-order rate constant, as determined from the logarithmic plots of CAT concentration *versus* time. To investigate the kinetic behaviour of the reaction, a double logarithmic plot of $(-dc/dt)$ against reactant concentration was analyzed, revealing the reaction order with reference to each reactant.

The progress of AgO nanoparticle catalyzed and uncatalyzed reactions were measured by the decay of CAT absorbance which observed in the absorption maxima (260 nm) (Fig. 1). The other constituents of reaction mixture were not absorbed in the same wavelength significantly. So, the computer controlled double beam spectrophotometer was used to determine the absorbance of the other constituents.

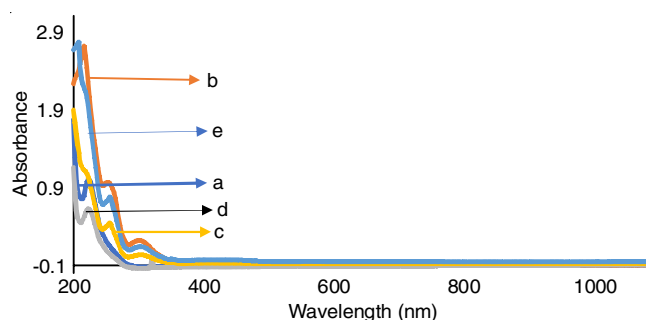


Fig. 1. Ultraviolet-visible spectra for various combinations of reactants: (a) [CAT] = 4×10^{-4} mol/L, (b) [oxcarbazepine] = 4×10^{-3} mol/L, (c) [CAT] = 4×10^{-4} and AgO nanoparticle catalyst = 0.001 g, (d) reaction mixture without nano catalyst [Cl⁻] = 2×10^{-3} mol/L, [HCl⁺] = 2×10^{-3} mol/L, (e) catalyzed reaction mixture [Cl⁻] = 2×10^{-3} mol/L, [HCl⁺] = 2×10^{-3} mol/L

Reaction stoichiometry and product identification:

Discrete set of reaction solution having OXC and AgO nanoparticle with an excess amount of CAT were thermodynamically equilibrated for about 48 h at 298 K. Kinetic experiments were conducted with an excess of CAT over OXC and the remaining unconsumed CAT confirmed a 1:1 stoichiometric

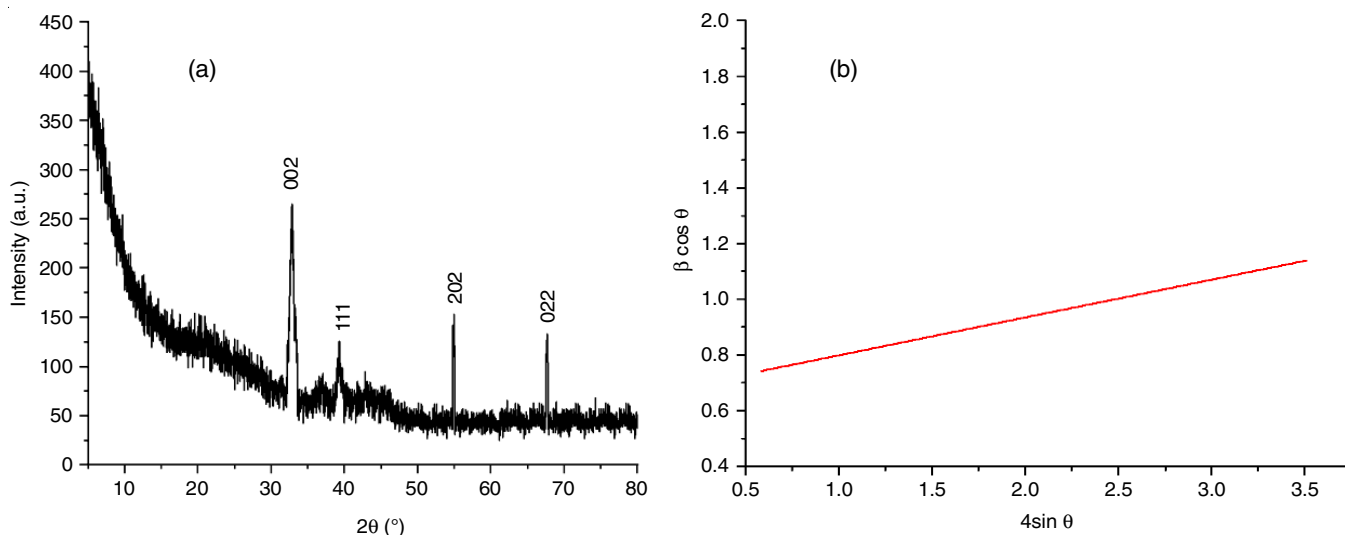
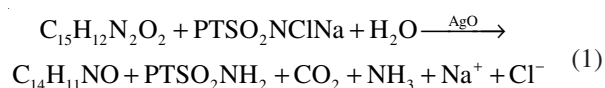


Fig. 2. XRD patterns of (a) AgO nanoparticle and (b) Williamson-Hall plot

ratio between CAT and OXC. Consequently, the stoichiometric was derived as follows:



where PT = $\text{CH}_3\text{C}_6\text{H}_4$.

The reaction yielded 5,11-dihydro-10*H*-dibezo[*b,f*]azepin-10-one as the predominant product. Diethyl ether was selected as the optimal extraction solvent for the recovery of the reaction product. The ether layer was then treated with aqueous NaOH solution, allowing the oxidation product of secondary amine substrate to be extracted and identified *via* spot test [25]. The compound was subjected to a nitrous acid test, which revealed the presence of a secondary amine group. *p*-Toluene sulfonamide (PTS), the reduction product of CAT, was extracted with ethyl acetate and identified by TLC using a solvent consisting of petroleum ether, chloroform and 1-butanol (2:2:1) and iodine as the visualizing agent ($R_f = 0.839$).

RESULTS AND DISCUSSION

Characterization of Silver Nanoparticles

X-ray diffraction: XRD was utilized to verify the content and crystallinity of the produced nanoparticles. Four distinct diffraction peaks at $2\theta = 32.86^\circ$, 39.75° , 55.02° and 67.69° can be correlated with the *hkl* values 022, 111, 202 and 022, respectively (Fig. 2a). These four peaks confirmed the existence of AgO in the sample, which is well-matched with the standard AgO JCPDS No. 84-1108. A detailed analysis of the crystallite size was performed using the Williamson-Hall (W-H) plot method Fig. 2b. The Williamson-Hall method provides a mathematical framework for understanding the XRD pattern broadening caused by micro strain, which is expressed as $\beta_s = 4\epsilon \tan \theta$, where β_s is the strain-induced broadening, ϵ is micro strain and θ is the Bragg angle. The crystallite size was subsequently approximated from the y-intercept/slope of linear fit, resulting in a value of 0.1355. The size of crystalline found to be 1.02 nm.

FTIR studies: FTIR spectroscopy was used to examine the interaction between biological molecules and composites during the synthesis of AgO nanoparticle, confirming the reduction and dispersion of chemical components. The prominent absorption peak at 616.22 cm^{-1} is observed in the spectrum (Fig. 3), which is attributed to the O-H stretching vibration of the amide group. The anti-symmetrical stretching vibration absorption of alkene double bonds was detected in the range, with significant peaks at 2024.73, 2185.17, 3752.23 and 3856.98 cm^{-1} .

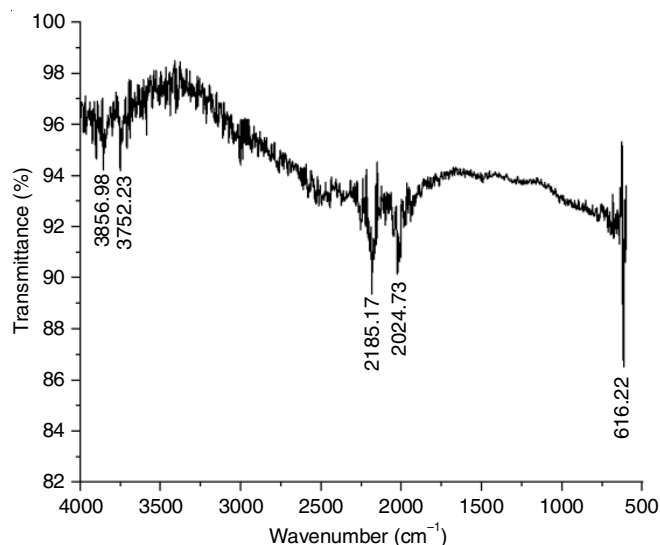


Fig. 3. FTIR spectrum of AgO nanoparticle

FE-SEM and EDX analysis were utilized to investigate the morphological and compositional properties of AgO nanoparticle: SEM analysis was employed to examine the morphology of the AgO nanoparticles, which revealed agglomeration of particles, while EDAX analysis provide valuable insights into their elemental composition. The EDAX spectrum (Fig. 4) clearly indicates the presence of AgO in the prepared sample as evidenced by the characteristic peaks. Table-1 pres-

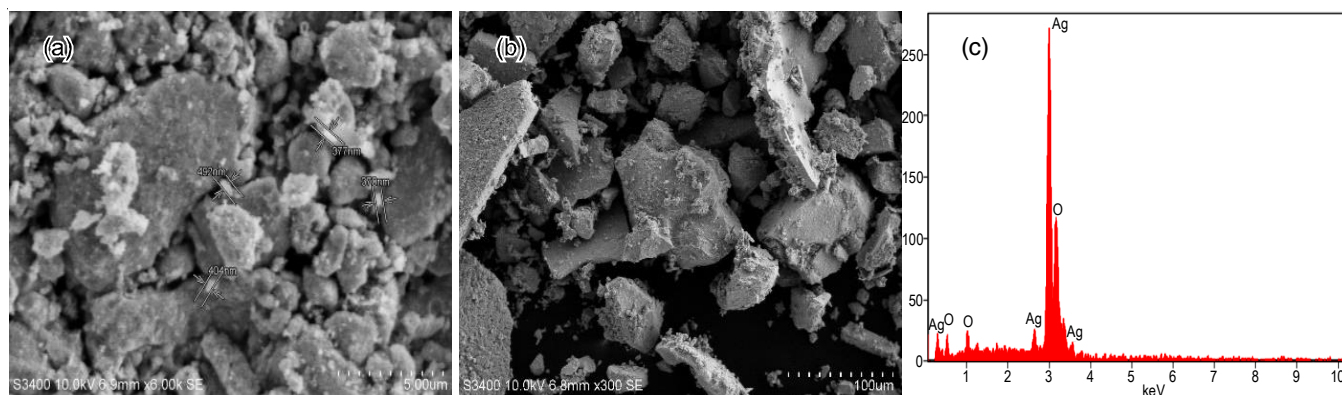


Fig. 4. SEM-EDX image of synthesized AgO nanoparticle

ents the comprehensive results of the SEM-EDAX analysis, including the detection of elements and their corresponding quantitative values, which are essential for understanding the properties of sample.

TABLE-1
STATISTICAL INFORMATION

Element line	Weight (%)	Weight (%) error	Atom (%)
O K	12.69	± 1.68	49.50
Ag L	87.31	± 3.06	50.50
Ag M	–	–	–
Total	100.00		100.00

Influence of variation of [oxidant] on the reaction rate:

In the course of pseudo-first order condition ($[OXC] \gg [CAT]$), kinetic runs been performed for both catalyzed and uncatalyzed oxidation of OXC in the presence of AgO nanoparticle by modifying $[CAT]$, at constant $[OXC]$, acid, AgO nanoparticle and temperature. The initial reaction rate was determined for each kinetic run. The method used was to draw a tangent to the

reaction progress curve at a fixed concentration of the oxidant (CAT). The slope of this tangent represents the initial rate of the reaction. At a fixed time point, a tangent was drawn to the curve. The pseudo-first order rate constant (k^1) was computed from the slopes. The constant k^1 values of uncatalyzed reaction with changing oxidant concentrations support the first-order dependance of the rate on $[CAT]_0$, whereas increasing k^1 values of the catalyzed reaction with increasing oxidant concentrations support the fractional order dependency on $[CAT]_0$.

$$k_1 = \frac{-(dc/dt)}{[CAT]}$$

Influence of substrate concentration variation on rate of reaction: By changing the $[OXC]_0$ concentration, the reactions were examined in comparable experimental settings. As $[OXC]$ increase, so as the k' values (Table-2). For both catalyzed and uncatalyzed processes, the fractional order dependence on $[OXC]_0$ is shown by the linear plot of $\log k'$ vs. $\log [OXC]_0$ (Fig. 5), with a fractional value of slope ($r = 0.3828$).

TABLE-2
IMPACT OF $[CAT]$, $[OXC]$, $[H^+]$, $[Cl^-]$ AND AgO ON THE OXIDATION OF OXCARBAZEPINE BY CHLORAMINE-T CATALYZED BY NANOPARTICLE IN AQUEOUS MEDIUM AT 298 K $\mu = 0.5$ mol/L, T 298 K, $10^3/D = 1.66$

$10^4 \times [CAT]$ (mol/L)	$10^3 \times [OXC]$ (mol/L)	$10^3 \times [HCl]$ (mol/L)	$10^3 \times [NaCl]$ (mol/L)	$10^3 \times AgO$ (g)	$10^4 \times k_u$ (S^{-1})	$10^4 \times k_c$ (S^{-1})	
						Observed	Calculated
2	4	2	2	2	2.49	4.55	4.54
4	4	2	2	2	2.40	4.57	4.52
6	4	2	2	2	2.48	4.59	4.53
8	4	2	2	2	2.46	4.53	4.57
4	4	2	2	2	2.49	4.53	4.52
4	6	2	2	2	3.00	5.27	5.26
4	8	2	2	2	3.58	5.97	5.92
4	10	2	2	2	4.00	6.39	6.31
4	4	2	2	2	2.49	4.53	4.53
4	4	4	2	2	2.63	5.11	5.12
4	4	6	2	2	2.79	5.67	5.64
4	4	8	2	2	3.37	6.13	6.12
4	4	2	2	2	2.49	4.53	4.52
4	4	2	4	2	2.21	3.63	3.62
4	4	2	6	2	2.00	2.39	2.38
4	4	2	8	2	1.89	1.98	1.96
4	4	2	2	2	–	4.52	4.53
4	4	2	2	4	–	4.87	4.83
4	4	2	2	6	–	5.12	5.15
4	4	2	2	8	–	5.64	5.65

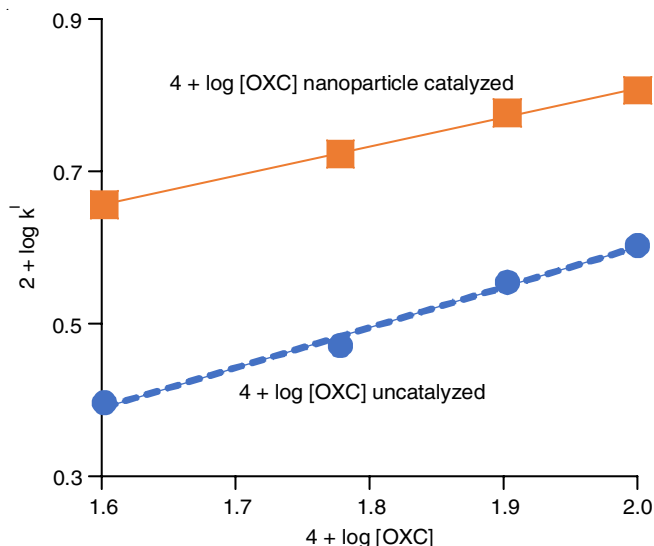


Fig. 5. Influence of substrate concentration on reaction rate at 298 K. [CAT] = 4×10^{-4} mol/L, [AgO] = 2×10^{-3} g

Influence of $[H^+]$ concentrations on reaction rate: In Fig. 6, both linear plots are parallel to each other, by maintaining the same concentration of substrate, oxidant and AgO nanoparticles, it is clarifying that the reaction of both uncatalyzed and nanoparticle-catalyzed reactions increases when the concentration of $[H^+]$ rises from 2×10^{-3} mol/L to 8×10^{-3} mol/L. For uncatalyzed and nanocatalyzed processes, respectively, the fractional order dependency of rate on $[H^+]$ is indicated by a linear plot of $\log k^1$ vs. $\log[H^+]$ with positive slopes of 0.22 and 0.216.

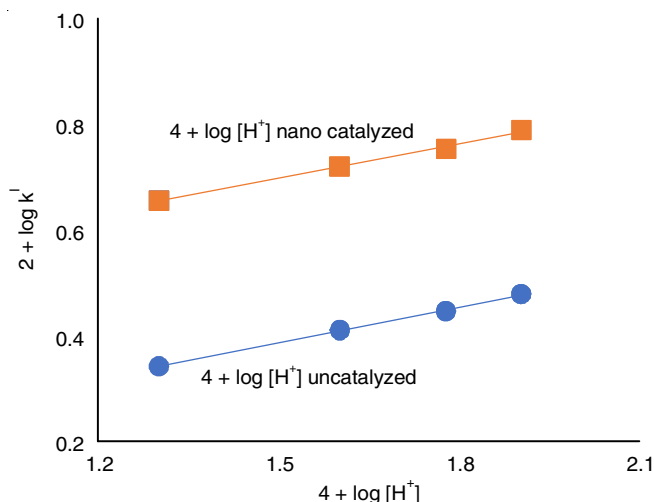


Fig. 6. Influence of $[H^+]$ on rate of reaction at 298 K. [CAT] = 4×10^{-4} mol/L, [AgO] = 2×10^{-2} g

Impact of reaction rate on the concentration of halide ions: Fig. 7 plot for uncatalyzed reaction shows that tangent line decreases on increasing [halide] from (4×10^{-3} mol/L – 8×10^{-3} mol/L) by keeping the other variables constant like substrate, acid and oxidant. In Table-2, while increasing in the $[Cl^-]$ ion the reaction rate gradually decreases. The slope value 0.197 and it is the negative fractional order dependence on $[Cl^-]$, as observed by the plot of $\log k$ against $\log [Cl^-]$.

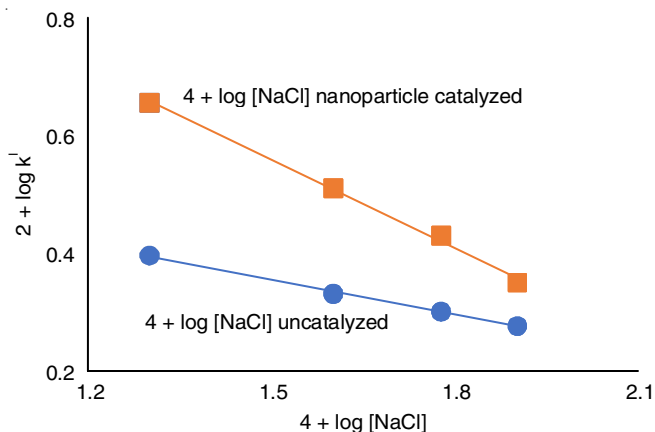


Fig. 7. Influence of halide ion concentration on reaction rate at 298 K. [CAT] = 4×10^{-4} mol/L, [AgO] = 2×10^{-3} g

In presence of AgO nanoparticles as catalyst, the concentration of chloride was varied by sustaining other parameters. Here also the rate of reaction decreases with increasing $[Cl^-]$. Fig. 7 shows both are parallel to each other and slope value 0.608 is greater than that of the uncatalyzed reaction indicate inverse fractional order dependence with $[Cl^-]$.

Ionic strengths influence on the rate: The influence of the ionic strength of medium on the rate was also investigated for both uncatalyzed and nanoparticle catalyzed processes by altering $[KNO_3]$ (0.1-1.0 mol/L) while leaving the other variable constant. The experiment reveals that there is no significant variance in the rate for both uncatalyzed and nanocatalyzed reactions. In both circumstances, the unchanged rate of reaction implies that non-ionic species are involved in the rate determining stage of the reaction.

Impact of dielectric permittivity on chemical reaction rate: In order to determine the effect of the dielectric permittivity on the rate of reaction, the rate was investigated *via* different dielectric constants (D) while keeping all other variables constant. The following equation describes the rate constant's dependency on the dielectric permittivity of medium.

$$\log k_1 = \log k_o - \frac{Z_A Z_B e^2 N}{2.303(4\pi\epsilon)d_{AB} RT} \times \frac{1}{D}$$

According to equation, the reaction rate constant (k_o) is influenced by factors such as ionic charges (Z_A and Z_B), temperature (T), dielectric constant (D) and the size of activated complex (d_{AB}). Methanol served as a solvent to examine the effect of dielectric permittivity (D) on the kinetics of catalyzed and uncatalyzed reactions. Table-3 indicates that rate decreases by increasing the proportion of dielectric permittivity of reaction for uncatalyzed and nanoparticle catalyzed reactions. A systemic study of the effect of dielectric constant on reaction kinetics was conducted by varying the methanol content (0-40%, v/v) in the reaction medium. The plot of $\log k^1$ vs. $1/D$ (Fig. 8) is linear with a downward slope. Blank experiments indicated that methanol was only slightly ionized (< 1%) under experimental conditions.

Kinetic analysis of influence of *p*-toluene sulfonamide on the reaction mechanism: Studies on the reduced product of *p*-toluene sulfonamide (PTS) reveal that changes in PTS

TABLE-3
EFFECT OF DIELECTRIC CONSTANT
IN MODULATING REACTION RATES

CH ₃ OH % (v/v)	D	10 ² (D ⁻¹)	k ¹ 10 ⁴ (sec)	k ¹ 10 ⁴ / (sec ⁴)
0	76.7	1.30	2.49	4.53
10	72.4	1.39	2.25	3.55
20	67.4	1.47	1.97	3.08
30	62.7	1.60	1.70	2.46
40	58.1	1.72	1.39	2.06

[CAT] = 4 × 10⁻⁴ mol/L, [AgO] = 2 × 10⁻³ g, [OXC] = 4 × 10⁻³ mol/L,
[H⁺] = 2 × 10⁻³ mol/L, μ = 0.5 mol/L, T = 298 K

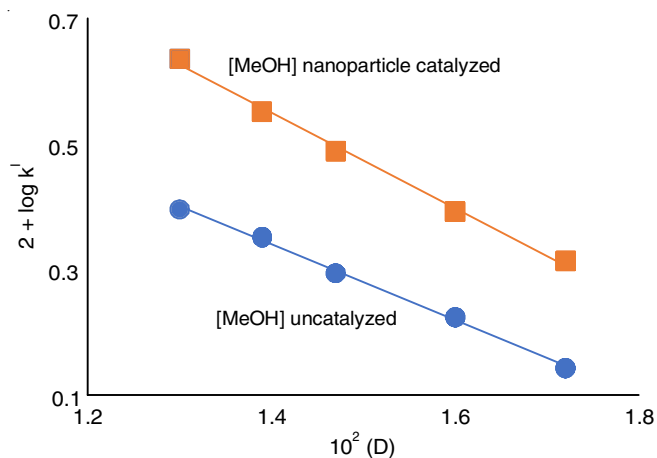


Fig. 8. Influence of dielectric permittivity on reaction rate

concentration (1 × 10⁻⁴ to 10 × 10⁻⁴ mol/L) do not significantly affect the reaction rate, indicating that PTS does not participate in the pre-equilibrium step for both the uncatalyzed and catalyzed reactions.

Temperature impact on reaction rate: To gain insight into the temperature-dependent kinetics of the reaction, a series of experiments were conducted at temperatures ranging from 293 to 313 K for both nanoparticle-catalyzed and uncatalyzed reaction. Table-4 reveals a systematic increase in the rate constant with rising temperature for both nanoparticle-catalyzed and uncatalyzed reactions. The linear Arrhenius plot depicted in Fig. 9 provides a visual representation of this trend, underscoring the significance of temperature in modulating the reaction kinetics. The kinetic and thermodynamic characteristics of the reaction was investigated by measuring the activation parameters for both reaction with and without nanoparticles.

TABLE-4
ACTIVATION PARAMETER AND TEMPERATURE-
DEPENDENT KINETICS OF OXC OXIDATION
CATALYZED BY CAT IN AQUEOUS ACID MEDIUM

Temp. (K)	k ¹ 10 ⁴ (sec ⁻¹)	k ¹ 10 ⁴ (sec ⁻¹)
298	2.00	4.01
303	2.49	4.53
308	2.70	5.32
313	4.08	6.57
318	5.00	8.59

[CAT] = 4 × 10⁻⁴ mol/L, [AgO] = 2 × 10⁻³ g, [OXC] = 4 × 10⁻³ mol/L,
[H⁺] = 2 × 10⁻³ mol/L, μ = 0.5 mol/L, 10²/D = 1.66

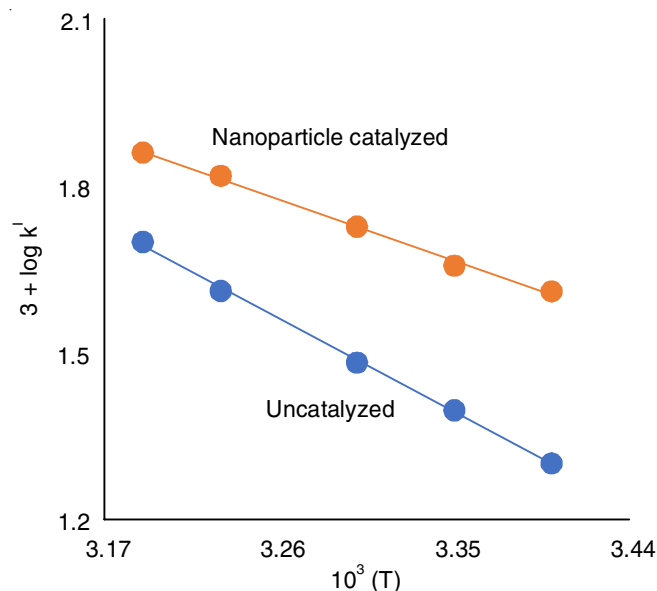


Fig. 9. Temperature dependence for uncatalyzed and nano catalyzed reaction

Thermodynamics parameters E_a , ΔH^\ddagger , ΔG^\ddagger and ΔS^\ddagger , evaluated from the Arrhenius plot in Table-5 favour proposed mechanism. A moderate value of E_a , ΔH^\ddagger , ΔG^\ddagger and a large negative value of entropy of activation, indicates the formation of compact complex intermediate which dissociates to give the product. These thermodynamic parameters have consideration lesser value for AgO nano-catalyzed reaction.

TABLE-5
THERMODYNAMIC PARAMETERS FOR UNCATALYZED
AND NANO CATALYZED REACTIONS

Thermodynamic parameters	Nanoparticle	
	Without	With
E_a (kJ mol ⁻¹)	25.43	22.33
ΔS^\ddagger (JK ⁻¹ mol ⁻¹)	-197.23	-203.627
ΔH^\ddagger (kJ mol ⁻¹)	22.99	19.90
ΔG^\ddagger (kJ mol)	82.78	79.56

Free radical detection and quantification: The uncatalyzed reaction mixture did not exhibit polymerization initiation when an aqueous solution of acrylamide was introduced. The absence of free radicle species in the uncatalyzed and catalyzed reactions is inferred from the lack of polymerization initiation. Conversely, the polymerization of nanoparticle-catalyzed reaction results demonstrate the absence of participation of free radicle species.

Mechanistic insights and rate law derivation: The uncatalyzed oxidation of OXC by CAT in aqueous medium exhibited a slow reaction rate. The stoichiometric analysis revealed a 1:1 mole ration between OXC and CAT, indicating that one mole of OXC reacts with one mole of CAT. The rate law was determined to be first-order in [CAT] and fractional-order in both [OXC] and [H⁺], suggesting a nonlinear dependence of the reaction rate on the concentrations of the reactants.

The mild oxidizing properties of CAT in both acid and alkali media are attributed to its ability to participate in a two-electron redox process, resulting in the formation of reduced products.

The electrolyte behaviour of CAT in aqueous solution is typical of a strong electrolyte, with complete ionization occurring upon dissolution. The acid-catalyzed hydrolysis of CAT in aqueous medium, is characterized by a complex series of equilibria, yielding a range of ionic species [25-29]:



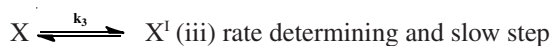
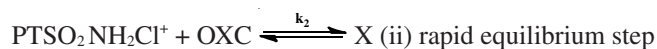
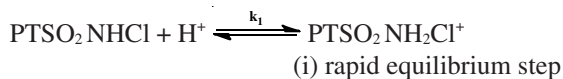
where PT = CH₃C₆H₄.

Consequently, PTSO₂NHCl, PTSO₂NCl₂ and HOCl are identified as the potential oxidizing species of CAT in aqueous acidic media. Since the rate does not exhibit second-order dependence on [CAT]₀, as indicated by eqn. 4, the possibility of PTSO₂NCl₂ acting as the reactive species was eliminated. Furthermore, the rate is not affected by the addition of *p*-toluenesulfonamide, which rules out a first-order retardation mechanism. As HCl is not primarily involved in the oxidation reaction, PTSO₂NHCl is considered the active oxidizing species. Under acidic condition (pH < 2), PTSO₂NHCl undergoes protonation to form the PTSO₂NHCl ion undergoes protonation to form the PTSO₂NH₂Cl⁺ ion [30,31].



At 298 K, the protonation constant for equilibrium (eqn. 7) was found to be 1.02 × 10². The observed retardation of the rate by added H⁺ ions supports the notion that deprotonation of PTSO₂NH₂Cl⁺ yields the active oxidizing species, PTSO₂NHCl.

To rationalize the experimental findings for the oxidation of OXC by CAT, **Scheme-I** is proposed. In this scheme, PTS₂NHCl is denoted as the active oxidant, OXC as the substrate and X and X^I as intermediate complex species. The present work provides a detailed mechanistic understanding of the reaction, which commences with the formation of PTSO₂NHCl. This species then reacts with the substrate to generate an intermediate complex X, which subsequently dissociates in the rate-determining step to yield the complex cation X^I, accompanied by the elimination of PTSO₂NH₂, shedding new light on the underlying reaction mechanism. Next, X^I reacts with water to form X^{II}, which then reacts with another molecule of PTSO₂NHCl to give the final products.



Scheme-I

Explicit rate equation is

$$\frac{d[\text{CAT}]}{dt} = k_3[\text{X}] \quad (8)$$

[CAT]_t is the effective total concentration of CAT

$$[\text{CAT}]_t = [\text{PTSO}_2\text{NH}_2\text{Cl}^+] + [\text{PTSO}_2\text{NHCl}] + [\text{X}] \quad (9)$$

$$[\text{CAT}]_t = \frac{[\text{PTSO}_2\text{NHCl}][\text{H}^+]}{k_1} + \frac{[\text{X}]}{k_2[\text{OXC}]} + [\text{X}] \quad (10)$$

After solving the X,

$$[\text{X}] = \frac{k_1 k_2 [\text{CAT}][\text{OXC}]}{[\text{H}^+] + k_1(1 + k_2)[\text{OXC}]} \quad (11)$$

$$\frac{d[\text{CAT}]}{dt} = \frac{k_1 k_2 k_3 [\text{CAT}][\text{OXC}]}{[\text{H}^+] + k_1(1 + k_2)[\text{OXC}]} \quad (12)$$

The rate law (eqn. 12) deduced from the mechanism agrees with experimental results, showing a first-order dependence on [CAT]₀, a non-integer order dependence on [OXC]₀ and an inverse fractional-order dependence on [H⁺].

It was stated that since the rate is equal to k^I [CAT]₀, eqn. 12 can be rearranged:

$$k^{\text{I}} = \frac{k_1 k_2 k_3 [\text{OXC}]}{k_1(1 + k_2)[\text{OXC}] + [\text{H}^+]} \quad (13)$$

$$\frac{1}{k^{\text{I}}} = \frac{1}{k_2 k_3 [\text{OXC}]} \left\{ \frac{[\text{H}^+]}{k_1} + 1 \right\} + \frac{1}{k_3 [\text{OXC}]} \quad (14)$$

Eqns. 13 and 14 suggest that the plots of 1/k^I against 1/[OXC] and 1/[H⁺] will yield linear relationships, enabling the determination of k₁, k₂ and k₃ from the slopes intercepts.

To investigate the effect of dielectric constant on the reaction, varying proportions (0-40%, v/v) of methanol were added to the medium. The resulting plot of log k^I versus 1/D revealed a negative dielectric effect, indicating the presence of dipole-dipole interactions.

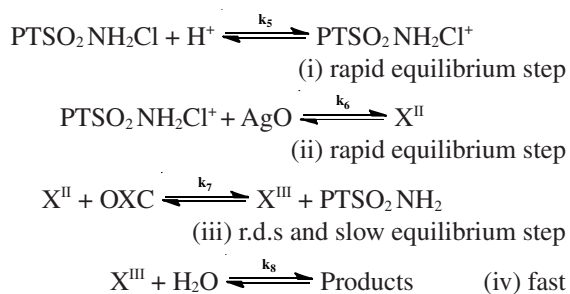
The rate remained unchanged upon addition of PTS, indicating its non-participation in the pre-equilibrium. Furthermore, the k^I versus 1/D plot exhibited a negative dielectric effect, implying significant dipole-dipole interactions. The invariance of the rate to changes in ionic strength implies that the rate-determining step is governed by non-ionic species [32-35]. A negative correlation between halide ion concentration and reaction rate was observed, suggesting a moderate inhibitory influence. Thermodynamic characteristics that align with the suggested mechanism, hence confirming the reaction pathway. A substantial loss of entropy is observed in the thermodynamic study of the transition state complex, which points to a compact, well-organized structure with limited degrees of freedom.

Kinetic analysis and rate law mechanism for nano-catalyzed processes: Based on kinetic data, the AgO nanoparticle-catalyzed oxidation of OXC by CAT in acidic aqueous medium is found similar stoichiometric features with the corresponding uncatalyzed reaction. The reaction rate exhibits first-order kinetics with respect to CAT. The kinetics of the reaction reveal a first-order relationship between the reaction rate and CAT concentration. The reaction rate goes up as the concentration of AgO nanoparticles increases, indicating fractional order kinetics. An increasing in [H⁺] ion concentration leads to an acceleration of the reaction rate, consistent with fractional

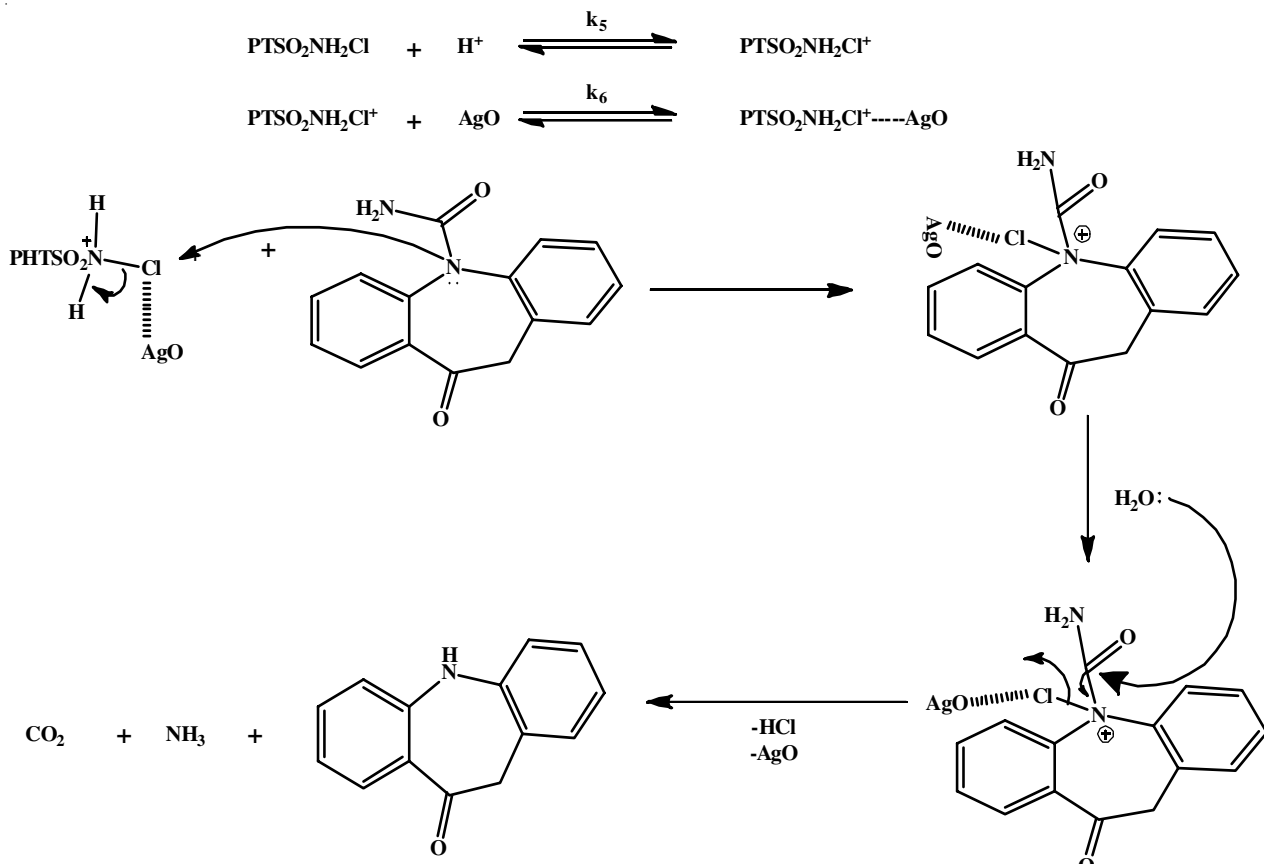
order kinetics. Furthermore, the effect of dielectric permittivity on the reaction rate was investigated, revealing a slightly positive slope, whereas the reaction exhibits negative entropy. This study provides an evidence that the observed fractional order dependence on [OXC] is a consequence of the complex formation between the substrate, CAT and the AgO nanoparticle catalyst in a pre-equilibrium step, which plays a crucial role in the reaction mechanism.



The reaction rate slows down when H^+ ions are added, which is likely due to the protonation of $\text{PTSO}_2\text{NH}_2\text{Cl}$, resulting in the formation of the protonated active oxidizing species $\text{PTSO}_2\text{NH}_2\text{Cl}^+$. A comprehensive analysis of the experimental results leads to the proposal of a reaction mechanism for the AgO nanoparticle-catalyzed oxidation of OXC by CAT, as illustrated in **Scheme-II**.



Scheme-II



Scheme-III

The active oxidant is represented by $\text{PTSO}_2\text{NH}_2\text{Cl}$ and the substrate is denoted by OXC. The catalyst reacts with CAT to form a precursor complex (X^{II}) before the slowest step in the reaction. The substrate OXC then combines with the previously formed complex in slow step of rate determining step generating intermediate X^{III} and PTSO_2NH_2 complex, while regenerating the AgO nanoparticle catalyst. Subsequent hydrolysis of the complex yields the desired products. The steps involved in the reaction are outlined in **Scheme-III**.

The differential rate equation is:

$$\frac{d[\text{CAT}]}{dt} = k_7[\text{X}^{\text{II}}] \quad (16)$$

where $[\text{CAT}]_t$ represents the effective total concentration of CAT,

$$[\text{CAT}]_t = [\text{PTSO}_2\text{NHCl}] + [\text{PTSO}_2\text{NH}_2\text{Cl}^+] + [\text{X}^{\text{II}}] \quad (17)$$

$$k_5 = \frac{[\text{PTSO}_2\text{NH}_2\text{Cl}^+]}{[\text{PTSO}_2\text{NHCl}][\text{H}^+]} \quad (18)$$

$$\text{PTSO}_2\text{NHCl} = \frac{[\text{PTSO}_2\text{NH}_2\text{Cl}^+]}{k_5[\text{H}^+]} \quad (19)$$

$$k_6 = \frac{[\text{X}^{\text{II}}]}{[\text{PTSO}_2\text{NH}_2\text{Cl}^+][\text{AgO}]} \quad (20)$$

$$\text{PTSO}_2\text{NH}_2\text{Cl}^+ = \frac{[\text{X}^{\text{II}}]}{k_6[\text{AgO}]} \quad (21)$$

$$\text{PTSO}_2\text{NHCl} = \frac{X^{\text{II}}}{k_6[\text{AgO}]} \quad (21)$$

$$\text{PTSO}_2\text{NH}_2\text{Cl}^+ = \frac{X^{\text{II}}}{k_5 k_6 [\text{AgO}][\text{H}^+]} \quad (22)$$

$$[\text{CAT}]_t = \frac{X^{\text{II}}}{k_5 k_6 [\text{AgO}][\text{H}^+]} + \frac{X^{\text{II}}}{k_6 [\text{AgO}]} + X^{\text{II}} \quad (23)$$

$$X^{\text{II}} = \frac{k_5 k_6 [\text{AgO}][\text{H}^+][\text{CAT}]_t}{1 + k_5 k_6 [\text{H}^+] + k_5 k_6 [\text{AgO}][\text{H}^+]} \quad (24)$$

Since rate = $k_7 [X^{\text{III}}]$

$$\text{Rate} = \frac{k_5 k_6 k_7 [\text{AgO}][\text{H}^+][\text{CAT}]_t}{1 + k_5 [\text{H}^+] + k_5 k_6 [\text{AgO}][\text{H}^+]} \quad (25)$$

A comparison between the deduce rate law and experimental result reveal excellent agreement, confirming the accuracy of the kinetic model.

$$\text{Reaction rate} = \frac{k_5 k_6 k_7 [\text{AgO}][\text{H}^+]}{1 + k_5 [\text{H}^+] + k_5 k_6 [\text{AgO}][\text{H}^+]}$$

On rearranging eqn. 25 we get

$$\frac{1}{k_c} = \frac{1}{k_7} \left\{ \frac{1}{k_6 [\text{AgO}]} \left(\frac{1}{k_5 [\text{H}^+]} + 1 \right) + 1 \right\} \quad (26)$$

Analysis of eqns. 25 and 26 reveals that linear plots of $1/k$ against $1/[\text{OXC}]$ and $1/[\text{H}^+]$ can be used to calculate the values of k_5 , k_6 and k_7 from the resulting slopes and intercepts. To modulate the dielectric constant of the medium, methanol was added in varying proportions (0-40%, v/v). The subsequent analysis of the $\log k^1$ versus $1/D$ plot demonstrated a negative dielectric effect, consistent with the presence of dipole-dipole interactions. The insensitivity of the reaction rate to the addition of *p*-toluene sulfonamide (PTS) suggests that it is not involved in the pre-equilibrium step. Moreover, the plot of k^1 versus $1/D$ revealed a negative dielectric effect, indicating the presence of dipole-dipole interactions in the reaction mechanism [31-33]. The reaction rate remained unchanged upon varying the ionic strength, indicating that the rate determining step involves non-ionic species. Moreover, the halide ions had a slight negative impact on the reaction rate. The computed thermodynamic parameters were in agreement with the proposed mechanism. The data indicates that the transition state is a rigid, compact complex with fewer degrees of freedom, which is consistent with the large negative entropy of activation and moderate positive values for free energy and enthalpy of activation.

Conclusion

A systemic comparative study was undertaken to investigate the oxidation of oxcarbazepine (OXC) by chloramine-T (CAT) in aqueous acidic medium, contrasting the effects of AgO nanoparticle catalyst and the absence of catalyst. We investigated the effectiveness of AgO nanoparticles as catalyst for the degradation of oxcarbazepine by CAT in acidic water. A detailed investigation of chloramine-T-OXC redox reaction in aqueous medium revealed a consistent 1:1 reaction stoichio-

metry, underscoring the mechanistic similarities between nanoparticle-catalyzed and uncatalyzed oxidation reactions. The resulting oxidation product was identified as 5,11-dihydro-10H-dibenzo[*b,f*]azepin-10-one. Furthermore, the influence of halide ions and dielectric permittivity on the reaction rate was systematically investigated. An analysis of the Arrhenius plots yielded the thermodynamic variables E_a , ΔH^\ddagger , ΔG^\ddagger and ΔS^\ddagger , which were evaluated using the observed kinetic parameters. A plausible mechanism has been proposed and the corresponding rate law has also been deduced. From the observed values, it was concluded that the green synthesis AgO nanoparticle exhibit potential activity during the oxidation of oxcarbazepine by chloramine-T.

ACKNOWLEDGEMENTS

The authors are indebted to the University of Mysore for resources and encouragement for this work.

CONFLICT OF INTEREST

The authors declare that there is no conflict of interests regarding the publication of this article.

REFERENCES

1. L.M. Bang and K. Goa, *Paediatr. Drugs*, **5**, 557 (2003); <https://doi.org/10.2165/00148581-200305080-00006>
2. S.J. Phelps and J.W. Wheless, *J. Pediatr. Pharmacol. Ther.*, **10**, 248 (2005); <https://doi.org/10.5863/1551-6776-10-4.248>
3. M. Zhou, N. Chen, L. He, M. Yang, C. Zhu and F. Wu, *Cochrane Libr.*, **2017**, CDD07963 (2017); <https://doi.org/10.1002/14651858.CD007963.pub3>
4. C.-W. Huang, C.-C. Huang, M.-W. Lin, J.-J. Tsai and S.-N. Wu, *Int. J. Neuropsychopharmacol.*, **11**, 597 (2008); <https://doi.org/10.1017/S1461145707008346>
5. M.M. Kalis, *Clin. Ther.*, **23**, 680 (2001); [https://doi.org/10.1016/S0149-2918\(01\)80019-9](https://doi.org/10.1016/S0149-2918(01)80019-9)
6. A. Musenga, M.A. Saracino, G. Sani and M. Raggi, *Curr. Med. Chem.*, **16**, 1463 (2009); <https://doi.org/10.2174/092986709787909604>
7. M.L. Chivers, M.C. Seto, M.L. Lalumière, E. Laan and T. Grimbos, *Arch. Sex. Behav.*, **39**, 5 (2010); <https://doi.org/10.1007/s10508-009-9556-9>
8. B.F. Bourgeois, *Epilepsia*, **41**, 1057 (2000); <https://doi.org/10.1111/j.1528-1157.2000.tb00297.x>
9. D. Carrozzino, D. Marchetti, D. Laino, M. Minna, M.C. Verrocchio, M. Fulcheri, A. Verrotti and P. Bech, *Nord. J. Psychiatry*, **70**, 424 (2016); <https://doi.org/10.3109/08039488.2016.1143029>
10. E. Kolvari, A. Ghorbani-Choghamarani, P. Salehi, F. Shirini and M.A. Zolfigol, *J. Iran. Chem. Soc.*, **4**, 126 (2007).
11. M.M. Campbell and G. Johnson, *Chem. Rev.*, **78**, 65 (1978); <https://doi.org/10.1021/cr60311a005>
12. D.S. Mahadevappa, K.S. Rangappa, B.T. Gowda and N.M.M. Gowda, *Microchem. J.*, **26**, 132 (1981); [https://doi.org/10.1016/0026-265X\(81\)90019-9](https://doi.org/10.1016/0026-265X(81)90019-9)
13. P. T. Sowmya, K.M. Lokanatha Rai, A. Sudhir and S.Y. Kotian, *Aust. J. Chem.*, **74**, 689 (2021); <https://doi.org/10.1071/CH21089>
14. G.L.S. Ferreira, P.L. Rosalen, L.R. Peixoto, A.L.A. de Lima Pérez, F.G. de Carvalho Carlo, L.R.C. Castellano, J.M. de Lima, I.A. Freires, E. de Oliveira Lima and R.D. de Castro, *Molecules*, **22**, 1527 (2017); <https://doi.org/10.3390/molecules22091527>
15. N. Rajendraprasad, K. Basavaiah and K.B. Vinay, *Int. J. Anal. Chem.*, **2011**, 138628 (2011); <https://doi.org/10.1155/2011/138628>

16. S. Malke, S. Shidhaye and V.J. Kadam, *Indian J. Pharm. Sci.*, **69**, 211 (2007);
<https://doi.org/10.4103/0250-474X.33145>
17. E. Kolvari, A. Ghorbani-Choghmarani, P. Salehi, F. Shirini and M.A. Zolfigol, *J. Iran Chem. Soc.*, **4**, 126 (2007);
<https://doi.org/10.1007/BF03245963>
18. D.S. Mahadevappa, S. Ananda, A.S. Murthy and K.S. Rangappa, *Tetrahedron*, **40**, 1673 (1984);
[https://doi.org/10.1016/S0040-4020\(01\)91116-0](https://doi.org/10.1016/S0040-4020(01)91116-0)
19. K.M. Meenakshi and K. Vasant Kumar Pai, *E-J. Chem.*, **6**, 545 (2009).
20. H.P. Jayadevappa and G. Nagendrappa, *Res. J. Chem. Sci.*, **3**, 3 (2013).
21. R. Ramachandrapa, *Res. J. Chem. Sci.*, **2**, 10 (2012).
22. A. Sukhdev, A.S. Manjunatha and P. Puttaswamy, *J. Int. Scholarly Res. Notices*, **1**, 2013 (2013);
<https://doi.org/10.1155/2013/738932>
23. Vidyasagar, R.R. Patel, S.K. Singh and M. Singh, *Mater. Adv.*, **4**, 1831 (2023);
<https://doi.org/10.1039/D2MA01105K>
24. V. Dhand, L. Soumya, S. Bharadwaj, S. Chakra, S. Bhatt and B. Sreedhar, *Mater. Sci. Eng. C*, **58**, 36 (2016);
<https://doi.org/10.1016/j.msec.2015.08.018>
25. F. Feig and V. Anger, *Spot Test in Organic Analysis*, Elsevier: Amsterdam, edn. 7, p. 376 (2005);
<https://doi.org/10.1016/C2009-0-07233-X>
26. P. Iyengar and R. Ramachandrapa, *Res. J. Chem. Sci.*, **2**, 7 (2012).
27. J.C. Morris, J.A. Salazar and M.A. Wineman, *J. Am. Chem. Soc.*, **70**, 2036 (1948);
<https://doi.org/10.1021/ja01186a016>
28. E. Bishop and V.J. Jennings, *Talanta*, **1**, 197 (1958);
[https://doi.org/10.1016/0039-9140\(58\)80034-X](https://doi.org/10.1016/0039-9140(58)80034-X)
29. F.F. Hardy and J.P. Johnston, *J. Chem. Soc., Perkin Trans. 2*, 742 (1973);
<https://doi.org/10.1039/p29730000742>
30. B.G. Pryde and F.G. Soper, *J. Chem. Soc.*, 1514 (1931);
<https://doi.org/10.1039/JR9310001514>
31. A. Sukhdev and P. Puttaswamy, *J. Springer Plus*, **2**, 30 (2013);
<https://doi.org/10.1186/2193-1801-2-30>
32. 28 D.K. Wolgemuth, S.D. Elmore, J.D. Cope, P.E. Sheridan, S.L. Stokes and J.P. Emerson, *Catal. Commun.*, **150**, 106275 (2021);
<https://doi.org/10.1016/j.catcom.2020.106275>
33. E.S. Amis, *Solvent Effects on Reaction Rates and Mechanism*, Academic Press: New York, p. 1672 (2007).
34. K.J. Laidler, *Chemical Kinetics*, Tata McGraw-Hill, New Delhi, edn. 3, p. 544 (2003).
35. J.H. Fagerberg, Y. Al-Tikriti, G. Ragnarsson and C.A.S. Bergström, *Mol. Pharmaceutics*, **7**, 1942 (2012);
<https://doi.org/10.1021/mp2006467>